JBC RESEARCH ARTICLE

The *Escherichia coli* RelB antitoxin C terminus is essential for RelE toxin suppression and transcriptional repression

Received for publication, May 15, 2025, and in revised form, June 10, 2025 Published, Papers in Press, June 18, 2025,
https://doi.org/10.1016/j.jbc.2025.110389

Julia Tanquary[1,2], **Ian J. Pavelich**[1], **Marcin Grabowicz**[3,4,5], **and Christine M. Dunham**[1,3,*]

From the [1]*Department of Chemistry, Emory University, Atlanta, Georgia, USA;* [2]*Graduate Program in Biochemistry, Cell and Developmental Biology, Graduate Division of Biological and Biomedical Sciences, Emory University, Atlanta, Georgia, USA;* [3]*Emory Antibiotic Resistance Center, Emory University, Atlanta, Georgia, USA;* [4]*Department of Microbiology & Immunology, Emory University School of Medicine, Atlanta, Georgia, USA;* [5]*Division of Infectious Diseases, Department of Medicine, Emory University School of Medicine, Atlanta, Georgia, USA*

Reviewed by members of the JBC Editorial Board. Edited by Karin Musier-Forsyth

Bacterial type II toxin–antitoxin (TA) systems exhibit high specificity within each pair to ensure precise recognition of the toxin by its cognate antitoxin to inhibit toxicity of the free toxin. Despite high structural similarity among some TAs, crosstalk between noncognate TA pairs is rare. To determine how the *Escherichia coli* RelB antitoxin suppresses its cognate RelE toxin, we engineered C-terminal truncations of RelB and tested their functional effects on toxin suppression in *E. coli*. We find that removal of the long C-terminal α3 and connecting loop 4 of RelB prevents RelE suppression. Quantitative binding assays of RelE and RelB variants support a reduced affinity upon removal of the RelB C terminus. Disrupting these interactions between RelB and RelE also led to a significant decrease in transcriptional repression at the *relBrelE* DNA operator (*relO*), underscoring the requirement for RelE binding to RelB for optimal repression at DNA repressor elements. Comparison to other structurally homologous TA systems, such as *E. coli* DinJ–YafQ, reveals key differences in the molecular mechanisms of both toxin suppression and DNA repressor activity highlighting the diversity in TA regulation and function.

Toxin–antitoxin (TA) systems are two-component genetic elements found throughout bacteria with many species encoding dozens of pairs (1–3). Discovered originally on plasmids and in prophages, these gene pairs are also found on chromosomes and were more recently identified adjacent to and contributing to CRISPR activity (4–9). After several decades of research identifying these unique modules, TAs are now classified into eight different types, distinguished by how the antitoxin suppresses its cognate toxin (3). In contrast to colicins, which are excreted to eradicate neighboring bacteria (10), TAs function within the host bacterial cell and are thought to regulate growth in a protective manner and to survive conditions of stress. Type II TA systems are the most abundant and well-characterized TAs, and a hallmark of these systems is that the antitoxin can function as transcriptional autorepressors, which control their expression in response to antitoxin proteolysis. This proteolysis causes toxins to accumulate, and their actions limit essential cellular processes and growth.

In type II TA systems, the ability of antitoxin proteins to recognize their cognate toxins is required to suppress toxic activity (3). Since there may be dozens of TA systems in each host organism, these TA interactions need to be specific and the binding between the pairs needs to occur with high affinity to sufficiently suppress the toxic phenotype of the toxin. In type II systems, in many cases, TAs exhibit low sequence identities (∼8–12%) especially among toxin proteins but can adopt similar tertiary structures. For example, the *Escherichia coli* DinJ–YafQ and RelB–RelE TA systems have ∼12% sequence identity between the YafQ and RelE toxins and ∼25% identity between their antitoxins, yet are structural highly similar (11) (Fig. 1). RelB–RelE is activated during amino acid starvation during the bacterial stringent response, whereas DinJ–YafQ is activated during oxidative and temperature stress (12–16). Both RelE and YafQ toxins are ribosome-dependent ribonucleases that cleave mRNA for degradation in the context of a translating ribosome to halt protein synthesis (17–20). In addition to the individual similarities between the RelE–YafQ toxins and RelB–DinJ antitoxins, both the RelB–RelE and DinJ–YafQ TA complexes adopt similar heterotetrameric architectures with each antitoxin C-terminal domain suppressing its cognate toxin by direct engagement (Fig. 1). RelB and DinJ antitoxins also contain ribbon–helix–helix motifs that recognize DNA repressor elements located within their own promoters, and antitoxin binding causes transcriptional repression during normal growth (11, 21–23).

The C terminus of DinJ wraps around the YafQ toxin interacting with YafQ at multiple sites to suppress YafQ toxicity (Fig. 2, *A* and *B*) (11, 23). Surprisingly, only the last nine amino acids of DinJ are required to fully suppress YafQ (24). Since the RelB antitoxin interacts with the RelE toxin in a very similar way, we tested the effect of RelB C-terminal truncations on its ability to bind and suppress its cognate RelE toxin. We find that, in contrast to the DinJ–YafQ TA complex,

* For correspondence: Christine M. Dunham, christine.m.dunham@emory.edu.

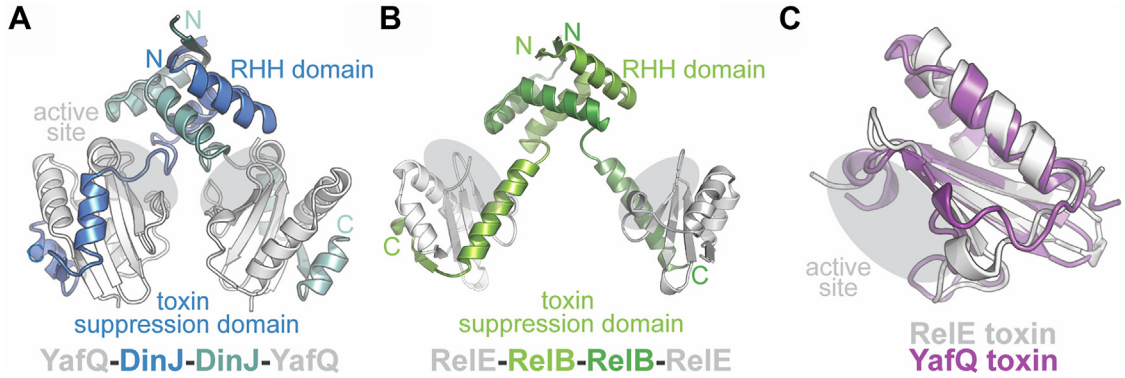

Figure 1. Comparison of the *Escherichia coli* DinJ–YafQ and RelB–RelE toxin–antitoxin systems. *A,* structure of the DinJ–YafQ heterotetrameric complex with the ribbon–helix–helix (RHH) motif and the toxin suppression domains of DinJ labeled and the active site of YafQ highlighted by a *gray oval* (Protein Data Bank [PDB] code: 4Q2U). *B,* structure of the RelB–RelE heterotetrameric complex with the RHH domain and toxin suppression domains of the RelB are labeled and the active site of RelE highlighted by a *gray oval* (PDB code: 4FXE). *C,* comparison of the RelE (*white*) (PDB code: 4FXI) and YafQ (*purple*) (PDB code: 4MI2) toxins with the toxin active site highlighted with a *gray oval*.

more extensive C-terminal truncations of RelB are required to decrease its interactions with RelE. In contrast to the DinJ–YafQ system, we also find that RelE binding to RelB is required for optimal transcriptional autorepression providing additional support for regulation of the *relBrelE* locus by a mechanism called conditional cooperativity (21, 22, 25, 26). Furthermore, assessing the protease accessibility of two loop regions in the RelB C terminus reveals these regions to be accessible *in vivo* in the context of the RelB–RelE TA complex, a similar finding in the DinJ–YafQ system (24). Together, these studies provide insights into differences between how structurally similar type II antitoxins suppress their cognate toxins and transcriptionally regulate their own expression.

Results

The C terminus of RelB is required to suppress RelE toxicity

The structure of the *E. coli* RelB–RelE complex revealed that the RelB antitoxin contains an N-terminal ribbon–helix–helix DNA-binding domain and a C-terminal domain that wraps around the RelE toxin, presumably to inhibit toxin function (21, 22, 27) (Fig. 1*B*). The complex exists as a heterotetramer with two RelE toxins and an obligate RelB dimer ($RelB_2$–$RelE_2$). Both RelB and RelE exhibit high structural homology to the *E. coli* DinJ antitoxin and YafQ toxin, respectively. Comparison of YafQ and RelE toxins (Protein Data Bank codes: 4Q2U and 4FXI) results in a Dali Z-score of 9.2 with an

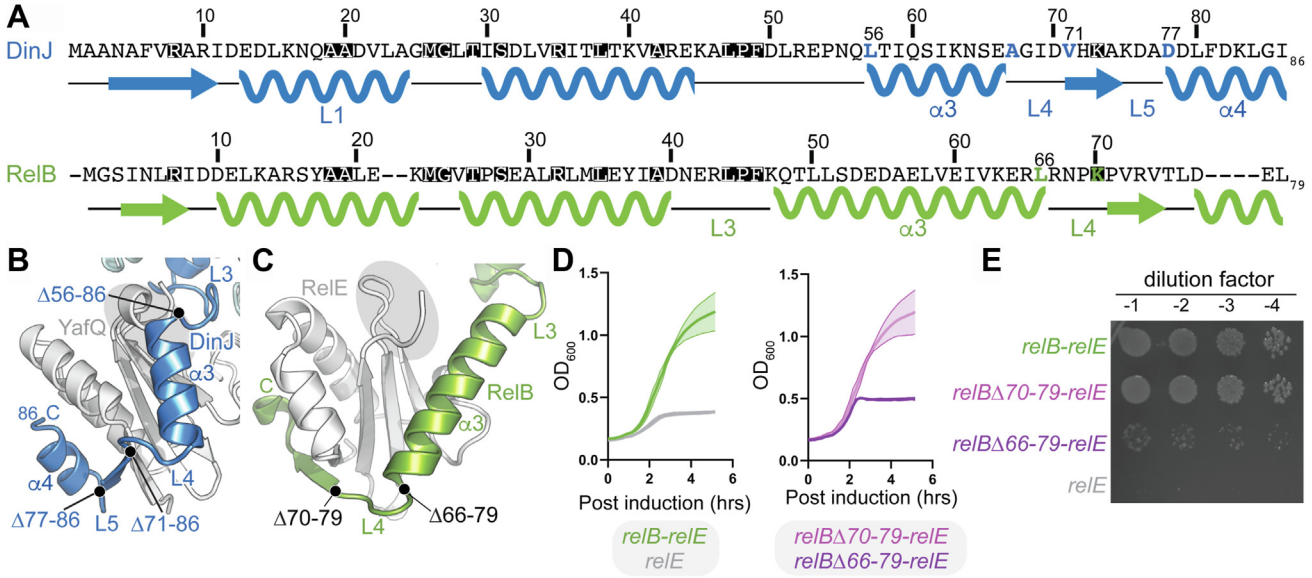

Figure 2. The RelB C terminus is essential for toxin suppression *in vivo*. *A, Escherichia coli* DinJ and RelB antitoxin sequence alignment with β-sheets and α-helices indicated with identical residues shown in *white* with a *black rectangle* and DinJ and RelB truncation residues shown in *bold* and in *color*. *B,* the DinJ–YafQ structure showing the YafQ toxin (*gray*) with the C-terminal toxin suppression domain of DinJ shown (*blue*; PDB code: 4Q2U). DinJ C-terminal truncations are indicated from a prior study (22). The YafQ active site is shaded *gray*. *C,* the RelB–RelE structure showing the RelE toxin (*gray*) with the toxin suppression domain of RelB shown (*green*; PDB code: 4FXE). RelB C-terminal truncations are indicated. The RelE active site is shaded *gray*. *D,* bacterial growth assays of *E. coli* BW25113 expressing RelB–RelE or RelE toxin only (*left*) and C-terminal truncated RelBΔ70–79–RelE or RelBΔ66–79–RelE variants. *Shaded region* represents mean ± SD of two experiments with three technical replicates each. *E, E. coli* BW25113 expressing RelB–RelE, RelBΔ70–79–RelE, RelBΔ66–79–RelE, or RelE toxin alone plated on LB supplemented with 0.2% arabinose (inducer). Agar growth represents efficiency of plating for a 10-fold dilution series of saturated culture. LB, lysogeny broth; PDB, Protein Data Bank.

alignment RMSD of 2.1 Å (Cα atoms), indicative of high structural similarity despite their low 12% sequence identity (11) (Fig. 1*C*). Both YafQ and RelE toxins adopt microbial ribonuclease folds and are ribosome-dependent ribonucleases that cleave mRNA actively undergoing protein synthesis on the ribosome (Fig. 1*C*) (17–20). DinJ and RelB antitoxins (Protein Data Bank codes: 4Q2U and 4FXE) are also structurally similar with a Dali Z-score of 5.1 and RMSD of 4.2 Å (Cα atoms) but have a higher sequence identity of ∼25% (11) (Fig. 2*A*). Similar to RelB–RelE, the DinJ–YafQ complex also adopts a hetero-tetrameric architecture with two YafQ toxins and an obligate DinJ dimer ($DinJ_2$–$YafQ_2$) (Fig. 1*A*). Both DinJ and RelB antitoxins inhibit their cognate toxins through interactions mediated by their C-terminal domains. Truncation of as few as nine amino acids of the DinJ C terminus inhibits DinJ–YafQ complex formation (Fig. 2, *A* and *B*) (24). Because of the structural similarity between the C termini of DinJ to RelB, we first designed analogous RelB truncations at solvent-accessible loop regions (Fig. 2, *A*–*C*). Free toxin from overexpression studies results in a bacterial growth defect, which we see when we overexpress RelE (Fig. 2*D*). Expression of both the RelE toxin and RelB antitoxin allows the antitoxin to suppress the toxin by direct binding, and normal growth resumes as seen for the RelB–RelE complex (Fig. 2*D*) (12, 25, 28–30). If truncated RelB is still able to bind to RelE, growth will continue, whereas any RelB truncations that disrupt this interaction will lead to inhibition of cell growth.

We truncated RelB at Lys70, which removes loop 4 (L4) and the terminal β-strand (RelBΔ70–79; Fig. 2, *A* and *C*). Removal of these nine C-terminal amino acids resulted in normal bacterial growth, similar to overexpression of RelB–RelE, indicating that the RelB–RelE interaction is retained (Fig. 2*D*). This result is in contrast to corresponding DinJ truncations where a comparably conservative truncation of DinJ disrupted interactions with the YafQ toxin, leading to impaired bacterial growth (24). We next removed L4 immediately after α3 by the insertion of a stop codon at Leu66 (RelBΔ66–79; Fig. 2, *C* and *D*). With this RelBΔ66–79 variant, growth is impaired but not as severely as when RelE alone is overexpressed (Fig. 2*D*). These strains had normal growth in the absence of inducer indicating that the growth phenotype was due to the inability of the RelBΔ66–79 variant to suppress RelE (Fig. S1*A*). To assess whether the RelB truncations led to its instability and thus a protein expression defect, we FLAG-tagged RelB–RelE, RelBΔ70–79–RelE, and RelBΔ66–79–RelE at the antitoxin N termini and performed immunoblot analysis. FLAG-RelBΔ70–79–RelE and FLAG-RelBΔ66–79–RelE are expressed comparably to FLAG-tagged RelB–RelE (Fig. S2). We also attempted other truncations at RelB residues 42, 43, 46, 57, and 75 in the context of the RelB–RelE construct, but these RelB variants have protein expression defects as assessed by immunoblot analysis, so we did not pursue these further.

We next compared the impact of RelBΔ70–79–RelE and RelBΔ66–79–RelE variants on cell viability *via* a spot dilution assay. When induced, RelB–RelE exhibits robust viability, indicating that RelE is suppressed by RelB; meanwhile, overexpression of RelE alone impairs growth almost completely (Fig. 2*E*). The RelBΔ70–79–RelE variant also exhibits robust viability, suggesting that an RelB–RelE complex still forms. The more extreme truncation of RelB, RelBΔ66–79–RelE, exhibits a severe impact on viability (Fig. 2*E*). *E. coli* harboring RelB–RelE, RelBΔ70–79–RelE, and RelBΔ66–79–RelE show normal growth in the absence of induction (Fig. S1*B*). Also, overexpression of RelBΔ70–79 and RelBΔ66–79 variants alone show normal growth indicating that expression of the RelB variants is not the cause for inhibition of growth (Fig. S1*C*). These studies indicate that L4 in RelB is likely important for stability of α3 (Fig. 2*C*), which directly contacts RelE. However, the absence of L4 could allow for more flexibility of the long α3, which could influence and reduce interactions between RelB and RelE. These results point to a more nuanced role of RelB suppression of RelE, which contrasts with what was previously observed in the structurally homologous DinJ–YafQ TA complex (11, 24).

RelB α3 and L4 mediate high-affinity RelE binding

We next sought to quantitatively characterize the impact of the RelB C-terminal Δ70–79 and Δ66–79 truncations on binding to RelE. TA complexes typically possess extremely tight binding affinities among cognate binding partners to suppress toxic activity from free toxin (2). For example, the *Streptococcus pneumoniae* PezA–PezT (31), *Mycobacterium tuberculosis* VapB–VapC11 (31), and *E. coli* RelB–RelE (26) TA pairs bind with subnanomolar affinities with K_d values of 0.065, 0.6, and 0.33 nM, respectively. To determine how the RelBΔ70–79 and RelBΔ66–79 truncations impact binding to RelE, we used a spectral shift approach to measure the change in emission fluorescence of the labeled RelE toxin simultaneously at two wavelengths upon binding with RelB variants. Although this approach has the advantage of requiring a small amount of protein for analysis, the lowest concentration of fluorescently labeled RelE, which could be detected, was 10 nM because of the detection limit of the instrument. Because this concentration is above the anticipated K_d for the RelB–RelE complex observed from prior published studies (26), we report our results as EC_{50}s rather than K_ds. We find that wildtype RelB binds to labeled RelE with an EC_{50} value of 2.6 nM indicating an extremely tight binding interaction (Fig. 3*A*; Table 1; confidence intervals [CIs] of 1.4–7.9 nM). Removal of the last nine amino acids of the RelBΔ70–79 variant, which removes the terminal β-strand, resulted in an EC_{50} of 880 nM, a >300-fold reduction in binding as compared with the wildtype RelB–RelE interaction (Fig. 3*B*; Table 1; CIs of 490–1600 nM). While the binding affinity between the RelBΔ70–79 variant and RelE is reduced, suppression of RelE toxin activity *in vivo* by RelBΔ70–79 is still observed as assessed by both growth assays and spot dilutions (Fig. 2, *D* and *E*). Removal of the last 13 C-terminal amino acids of RelB (RelBΔ66–79), which in addition removes L4 immediately after α3, further reduced binding to an EC_{50} of 24 μM, which is a >9000-fold reduction as compared with wildtype RelB–RelE interaction (Fig. 3*C*; Table 1; CIs of

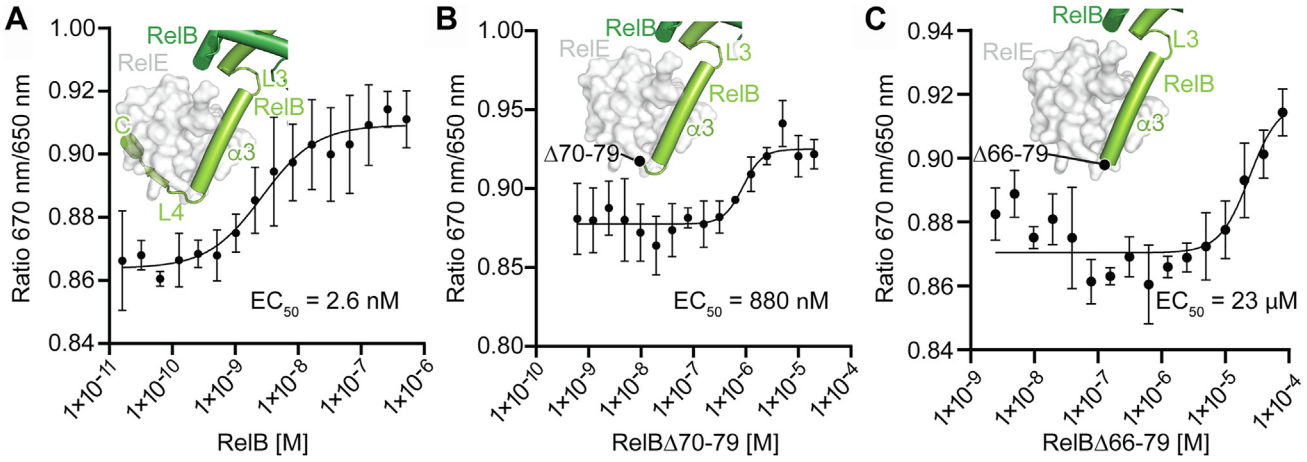

Figure 3. Essentiality of the RelB C terminus for binding to RelE. Spectral shift assays were used to determine the binding affinity of wildtype RelB, RelBΔ70–79, or RelBΔ66–79 to labeled RelE. *A–C*, fitted curves and calculated binding EC_{50}s are shown. Error bars represent the SD of two technical replicates from two different protein preparations.

13–400 μM). These data show a significant reduction in binding between RelBΔ66 and 79 to RelE and are consistent with a significant decrease in cell growth and viability with the interpretation being that RelE is no longer suppressed by RelBΔ66–79. Collectively, these data indicate the importance of the RelB L4 in potentially tethering the long α3 helix to RelE resulting in its suppression. In the absence of L4, α3 may exhibit more flexibility that significantly reduces RelE binding.

Requirement of RelE binding to RelB for optimal transcriptional repression at relO

Type II TA complexes like RelB–RelE bind at operator regions that overlap with their promoter to repress transcription during normal growth (21, 25, 26). RelB transcriptionally represses *relBrelE* expression by binding at a single *relBrelE* DNA operator (*relO*), which overlaps with the −10 region of the promoter (Fig. 4*A*). This regulation is modulated by varying molar ratios of RelB and RelE *via* a mechanism termed conditional cooperativity (2, 25, 32–34). While the RelB dimer alone can bind at *relO*, the strength of binding *relO* is increased upon RelE toxin binding to RelB (25, 30). However, excess RelE toxin binding at RelB–*relO* has been proposed to cause a conformational change of the TA complex that reduces its affinity for *relO* and causes derepression (22, 30, 35). To understand how RelBΔ70–79–RelE and RelBΔ66–79–RelE variants affect this transcriptional regulatory mechanism as a function of the strength of the RelB–RelE complex, we performed reporter assays. Transcriptional fusions using β-galactosidase (β-gal) and GFP as reporter fusions are commonly used to study the effects of TA complexes on transcriptional repression *in vivo* (11, 24, 36–39). The *relBrelE* promoter including *relO* where RelB–RelE binds was cloned before *lacZ* into pOU254, a low copy, promoter-less plasmid previously used in TA biology (25, 40). *E. coli* BW25113 were cotransformed with pOU254–*relO* and either RelBΔ70–79–RelE or RelBΔ66–79–RelE constructs, similar to the constructs used in growth and spot dilution assays (Fig. 2, *D* and *E*). We used the RelE–R81A variant, which was shown to reduce RelE toxicity in an attempt to reduce the effect of RelE toxicity on cell growth (30, 41) (Fig. S3*A*). We find that the RelE–R81A variant does not display a growth defect within the time frame of the reporter assay (Fig. S3*A*).

Using the transcriptional reporter assay, we find that RelB–RelE–R81A display low levels of β-gal activity, indicating transcriptional repression at *relO* by their binding (Fig. 4*B*; Fig. S3*B*). We report this as 100% transcriptional repression at *relO*, and all subsequent β-gal experiments are normalized to RelB–RelE–R81A (Fig. 4*B*). Expression of RelBΔ70–79–RelE–R81A also shows robust transcriptional repression similar to RelB–RelE–R81A (Fig. 4*B*). Truncating RelB at L4 (*i.e.*, RelBΔ66–79–RelE–R81A) results in ∼2.3-fold decrease in Miller units, which corresponds to ∼26% transcriptional repression as compared with RelB–RelE–R81A (Fig. 4*B*). These results indicate that tight RelE binding to RelB contributes to repression at *relO*. We further verified the levels of the *lacZ* transcripts by RT–quantitative PCR (qPCR) (Fig. 4*C*). In *E. coli* BW25113 expressing only pOU254–*relO*, we observed robust levels of *lacZ*, an ∼11-fold increase as

Table 1
Binding interactions (EC_{50}) of RelB and RelB C-terminal truncations to RelE

Variant	EC_{50}	Fold change	CI (M)	Hill slope
RelB	2.6×10^{-9} M (2.6 nM)		1.4×10^{-9}–7.9×10^{-9} (1.4–7.9 nM)	1.0
RelBΔ70–79	8.8×10^{-7} M (880 nM)	338	4.9×10^{-7}–1.6×10^{-6} (490–1600 nM)	2.4
RelBΔ66–79	2.4×10^{-5} M (24 μM)	9230	1.3×10^{-5}–4.0×10^{-4} (13–400 μM)	1.9

The binding affinity of wildtype RelB or RelB C-terminal truncations to labeled RelE was determined *via* spectral shift. EC_{50}, CIs, and the Hill slope for each reaction were determined from two technical replicates of two different protein preparations. Fold change comparing the binding interaction between RelB C-terminal truncations and RelE to the binding interaction between full-length RelB and RelE was determined.

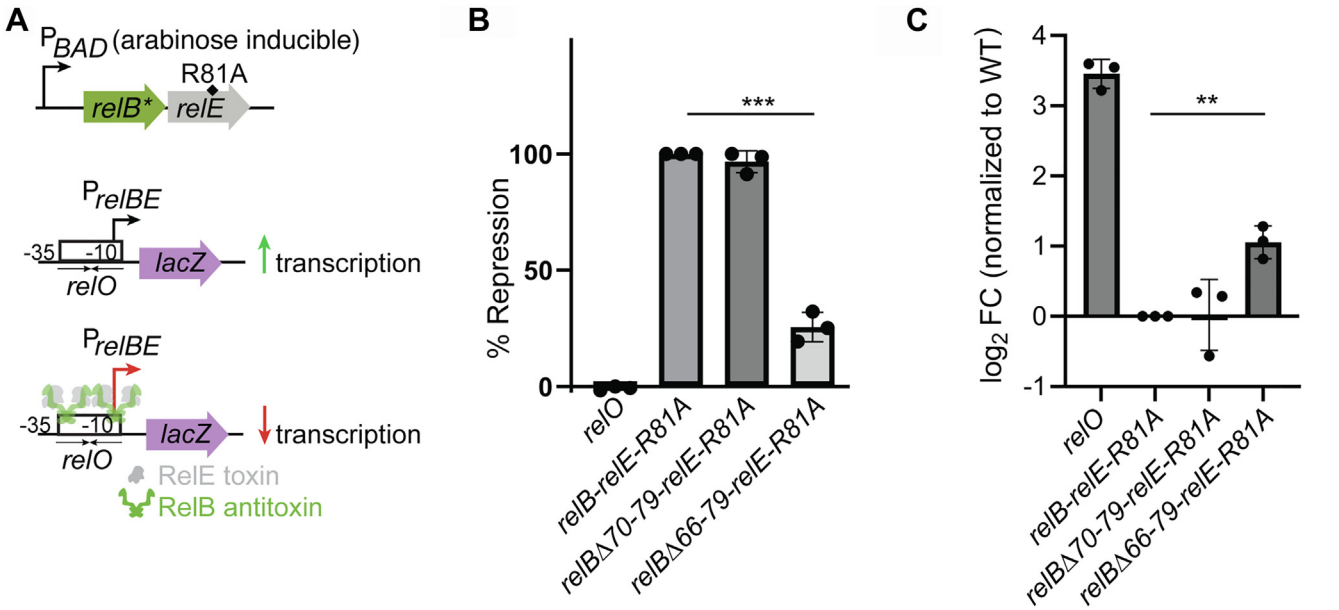

Figure 4. RelB C-terminal truncations reduce transcriptional repression at *relO*. *A,* schematic of plasmids used in β-gal activity assays to test transcriptional repression at *relO* by RelB C-terminal truncations. The *relO* promoter was inserted before *lacZ*, which results in full transcriptional activity. Expression of the wildtype RelB–RelE–R81A, RelBΔ70–79–RelE–R81A, or RelBΔ66–79–RelE–R81A was tested for repression at the *relO* operator 1 site that overlaps with the −10 promoter region. *B,* β-gal assays plotted as a function of transcriptional repression of *Escherichia coli* BW25113 expressing pOU254–*relO* and RelB–RelE–R81A, RelBΔ70–79–RelE–R81A, or RelBΔ66–79–RelE–R81A. Percent transcriptional repression is defined as a decrease in β-gal activity levels from cells lacking plasmid-encoded RelB or RelE, normalized to wildtype RelB–RelE–R81A. Error bars are mean ± SD of three experiments with three technical replicates each. Significance in the percent repression was determined by an unpaired *t* test ($p < 0.0001$). *C,* expression of *relB–relE–R81A-lacZ, relBΔ70–79–relE–R81A-lacZ,* or *relBΔ66–79–relE–R81A-lacZ* was measured by RT–quantitative PCR. Log_2 fold change was calculated *via* the ΔΔCT method and *relBΔ70–79–relE–R81A-lacZ* or *relBΔ66–79–relE–R81A-lacZ* expression was normalized to *relB–relE–R81A-lacZ*. Error bars are mean ± SD of three biological replicates with three technical replicates each. Significance in log_2 fold change was determined by an unpaired *t* test ($p < 0.001$). ** represents $p < 0.05$ and *** represents $p < 0.001$. β-gal, β-galactosidase.

compared with *E. coli* BW25113 expressing wildtype RelB–RelE–R81A (Fig. 4*C*). Consistent with our β-gal assays, both RelB–RelE–R81A and RelBΔ70–79–RelE–R81A expressed low levels of *lacZ* because of transcriptional repression. We also observed that *lacZ* expression when RelBΔ66–79–RelE–R81A is expressed causes a ∼2-fold increase in *lacZ* transcript levels as compared with RelB–RelE–R81A. These results show that preventing RelE binding to RelB by severely truncating the RelB C terminus directly prevents transcriptional repression at *relO* and causes derepression.

RelB loops L3 and L4 are accessible to proteolysis in vivo

One possible mode of activation of type II toxins is the proteolysis of solvent-accessible regions in the antitoxin by specific cellular proteases (12, 24, 26, 42). Loops 3 and 5 (L3 and L5) in DinJ are accessible to proteolytic cleavage, and L5 is an *in vitro* substrate of Lon protease, a protease that degrades DinJ and RelB *in vivo* (19, 24, 26). Guided by these results that show L3 and L5 of DinJ are accessible to proteolysis by tobacco etch virus (TEV) protease, we sought to determine if L3 and L4 of RelB are also accessible to cellular proteases. We introduced the TEV protease recognition sequences into L3 or L4 and coexpressed either RelB-L3-TEV–RelE or RelB-L4-TEV–RelE variants with a plasmid encoding TEV protease (Fig. 5). Expression of TEV, RelB-L3-TEV–RelE, or RelB-L4-TEV–RelE alone do not result in a growth defect (Fig. S4). Expression of both RelB-L4-TEV–RelE and TEV protease results in a slight reduction in growth (Fig. 5*B*). Further inhibition of growth is seen in the RelB-L3-TEV–RelE variant when coexpressed with TEV (Fig. 5*B*). These data suggest that both L3 and L4 in RelB are cleaved by TEV resulting in free RelE that reduces growth with L3 appearing to be more accessible because this variant exhibits a further reduction in growth. We further verified that TEV overexpression results in cleavage of RelB-L4-TEV and RelB-L3-TEV using mass spectrometry (Fig. S5). TEV proteolysis does occur at L3-TEV or L4-TEV, but proteolysis is not complete, consistent with the minor growth defect. These data suggest that RelB L3 and L4 may be substrates for cellular proteases that act on RelB to activate RelE and further underscore the importance of α3 in RelB for RelE suppression.

*Differences in predicted structures of DinJ–YafQ–DinJ DNA repressor element and RelB–RelE–*relO *DNA repressor element*

Structures of TA complexes bound to DNA operators have provided important insights of structural rearrangements that may need to occur upon DNA binding (43). However, no structures exist of the DinJ–YafQ–*dinJ* complex or the RelB–RelE–*relO* complex. We used AlphaFold 3 (AF3) (44) to predict the structures of DinJ–YafQ and RelB–RelE bound to single inverted repeats (IRs) of *dinJ* and *relO*, respectively (Fig. 6*A*). The predicted DinJ–YafQ–IR1 complex reveals little to no conformational changes of DinJ–YafQ upon recognition of *dinJ* as compared with the apo DinJ–YafQ structure (11, 23)

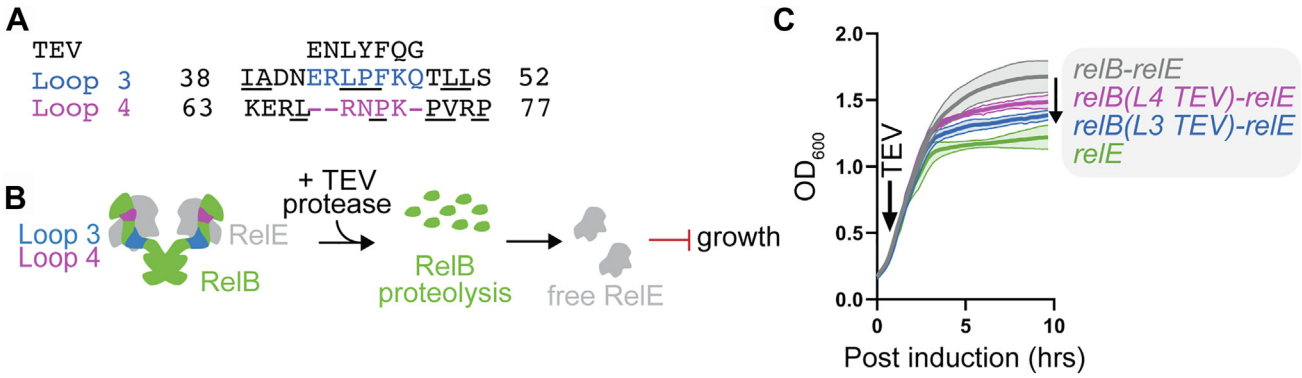

Figure 5. Loops 3 (L3) and 4 (L4) of RelB are accessible to proteolysis by TEV protease. *A,* amino acid sequence of RelB L3 (*blue*) and L4 (*purple*) that were substituted with the TEV protease recognition sequence shown at *top*. Hydrophobic residues in L3 and L4 are *underlined*. *B,* schematic of assay to determine accessibility of RelB loops to TEV protease. RelB (*green*) with TEV protease recognition sequence at RelB L3 (*blue*) and L4 (*purple*). *C,* bacterial growth assays of *Escherichia coli* BW25113 expressing TEV and RelB–RelE, RelB-L3-TEV–RelE, RelB-L4-TEV–RelE, or RelE only. Overexpression was induced at time 0, and TEV expression or RelE was induced at 1.5 h. *Shaded regions* are mean ± SD of two experiments with three technical replicates. TEV, tobacco etch virus.

(Fig. 6*A*; Fig. S6). The AF3 ranking score of DinJ–YafQ–*dinJ* is 0.94 revealing high confidence in this model. For the RelB–RelE–*relO* prediction, we obtained two different predicted structures, both of which differ significantly from the free RelB–RelE complex (Fig. 6, *B* and *C*; Fig. S6) (22). The AF3 ranking scores for these two models are lower (model 1—0.54; model 2—0.68) revealing lower confidence in both models. Both predicted models show substantially different conformational changes of the RelB–RelE complex as compared with free RelB–RelE complex. An additional difference between these two models is in the orientation of the long α3. In model 1, α3 is closer to *relO*, and the two RelEs are predicted to interact with each other (Fig. 6*B*). In model 2, α3 is oriented away from *relO*, and RelE interacts with both RelB and *relO* (Fig. 6*C*).

Discussion

To determine how two structurally homologous TA pairs form complexes capable of suppressing toxin activity and permits optimal transcriptional repression at their DNA repressor elements, we studied the *E. coli* RelB–RelE TA system and directly compared our findings to the DinJ–YafQ complex (24). We anticipated that removal of a short segment of the C terminus of RelB would prevent RelE binding, similar to what we observed with DinJ C-terminal truncations (24). However, despite the very similar structures of these two TA complexes, a significantly larger RelB truncation is needed to ablate its interaction with RelE *in vivo*: removal of the analogous last nine amino acids in RelB (RelBΔ70–79) to that of the DinJ (DinJΔ77–86) sustained bacterial growth indicating that the RelB–RelE complex was maintained and

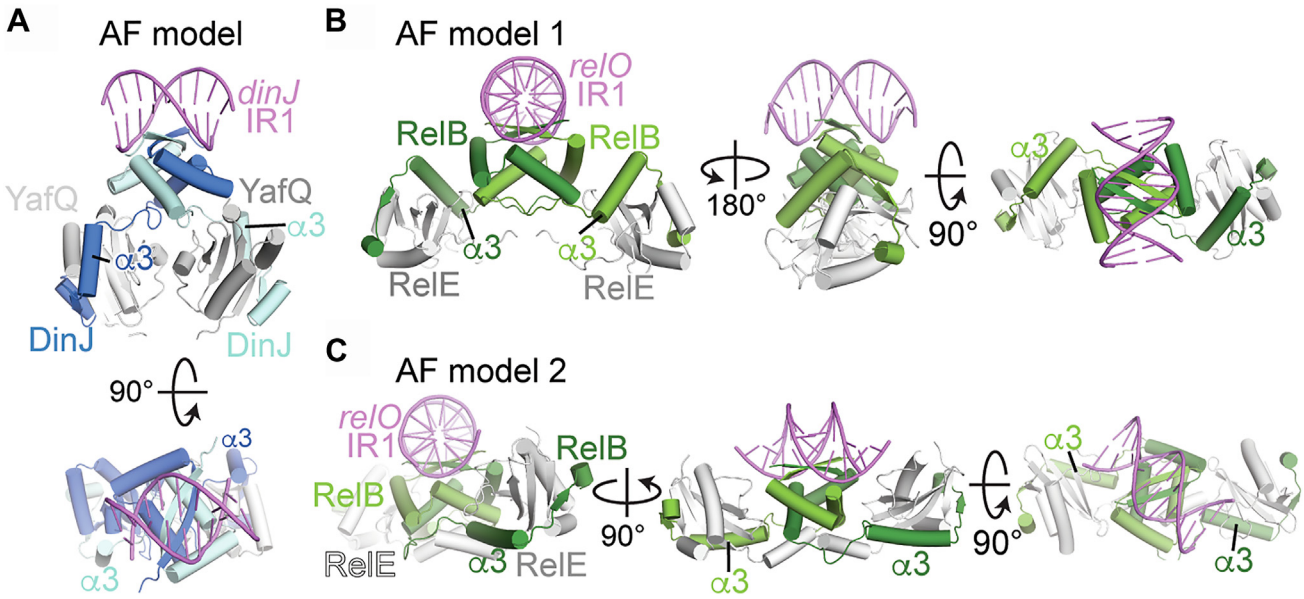

Figure 6. AF3 models of DinJ–YafQ–*dinJ* and RelB–RelE–*relO*. *A,* AF3 model of DinJ–YafQ (PDB code: 4Q2U) interacting with a single inverted repeat of *dinJ* (ranking score of 0.94). *B* and *C,* two AF3 models of RelB–RelE (PDB code: 4FXE) interacting with a single inverted repeat of *relO* differ in how they interact with *relO*. Ranking score for AF3 model 1 is 0.54 and for model 2 is 0.68. AF3, AlphaFold 3; PDB, Protein Data Bank.

thus RelE was suppressed. Quantitative binding studies between RelBΔ70–79 and RelE indicate that while the interaction strength is decreased by more than 300-fold (from 2.6 to 880 nM), the strength of the binding interaction remains sufficiently high enough so that there is still RelE toxin suppression by the RelBΔ70–79 variant *in vivo*. In contrast, removal of the RelB L4 (RelBΔ66–79) results in a significant decrease in cell growth and viability and a >9000-fold decrease in binding affinity (24 μM). Therefore, the four residues of L4 seem to be especially important in mediating specific interactions between RelB and RelE, in contrast to the DinJ–YafQ system where the C-terminal α4 of DinJ is the main mediator of the interactions with the YafQ toxin.

In the context of binding the YafQ toxin, the C-terminal α4 of DinJ buries many hydrophobic residues that likely stabilizes this interaction (Fig. S7). We previously predicted that this six-residue hydrophobic patch was important for stabilizing these interactions in the DinJ–YafQ complex, but these studies lacked quantitative binding assays to confirm this (24). Although a similar buried hydrophobic patch exists between RelB (Val72, Val74, Leu76, and Leu79) and RelE (Leu5, Pro7, Leu12, Leu30, and Val31) (Fig. S7), this hydrophobic interaction does not seem to be as critical for the RelB–RelE complex because removal of these contacts (RelBΔ70–79) still results in both *in vivo* toxin suppression and a sufficiently high-affinity binding interaction. Thus, other RelB components could also provide additional contributions to the recognition and binding of RelE. One type II TA system that contains many multiple TA surfaces that result in partial toxin suppression is the *Salmonella enterica* serovar Typhimurium TacT–TacA system (45). In this system, there appears to be one primary antitoxin binding interface that is sufficient for cognate toxin neutralization, but other interfaces distant from the TacT–TacA interface were found to partially compensate when the main binding interface was disrupted as assessed by bacterial growth (45). This system seems to be distinct from the RelB–RelE system because multiple TacA antitoxins bind to a single TacT toxin, whereas there appears to be one primary interface in the RelB–RelE system with only one RelB antitoxin binding to one RelE toxin.

Potential reasons for the differences in toxin suppression between the DinJ–YafQ and RelB–RelE TA systems are the length of the loop that connects the N and C termini of both the RelB and DinJ antitoxins and the resulting width of the complexes (Fig. 7). In RelB, the L3 that connects its N and C terminus is shorter than the L3 in DinJ (five *versus* nine residues), which restricts the orientation of its long α3. We predict that this restriction stabilizes α3 packing against RelE. Comparison of the angle between the N and C termini of RelB and the corresponding angle in DinJ reveals a significant increase (60° *versus* 37°), which widens the overall RelB–RelE tetramer (Fig. 7B). This widening has mechanistic implications because it influences how the RelB–RelE complex interacts with *relO* and how the system is responsive to excess RelE toxin binding (22) (Fig. 7B). Binding of additional free RelE toxin is predicted to result in steric clashes between two RelEs bound at $RelB_2$–*relO*, which, in turn, induce conformational changes that cause derepression (22). The RelB–RelE tetramer is wider than the DinJ–YafQ tetramer (77.7 Å *versus* 64.2 Å), which we propose influences how each TA system engages its DNA repressor element to regulate transcriptional repression. Since the DinJ–YafQ system does not appear to be regulated by excess YafQ toxin *via* conditional cooperativity (11, 20, 24), this may be because the DinJ–YafQ footprint is smaller than RelB–RelE, and this smaller footprint then prevents clashing between other DinJ–YafQ complexes bound at an adjacent DNA operator site. Interestingly, AF3 modeling of RelB–RelE–*relO* and DinJ–YafQ–*dinJ* predicts striking differences in how each

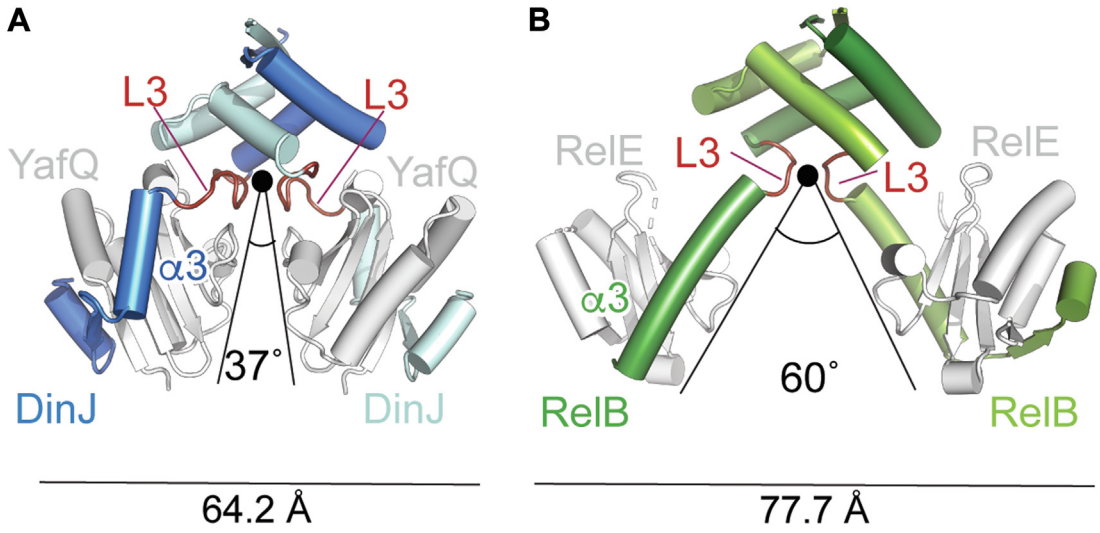

Figure 7. Structural differences of DinJ–YafQ and RelB–RelE that likely influence its interactions with its DNA repressor element. *A,* comparison of DinJ–YafQ (PDB code: 4Q2U) and RelB–RelE (PDB code: 4FXE) (*B*) highlight differences in loop 3 (L3; *red*) that likely influences the location of the α3 in both DinJ and RelB. Both L3 and α3 influences the overall TA complex. In DinJ–YafQ, these elements narrow the overall complex (*e.g.*, 64.2 Å) as compared with the RelB–RelE complex, which is widened (*e.g.*, 77.7 Å). PDB, Protein Data Bank; TA, toxin–antitoxin.

TA likely interacts with its DNA repressor element, which we predict may lead to the key differences seen in transcriptional regulation (Fig. 6).

Transcriptional repression at TA loci including *relO* can be mediated by potential changes of TA levels, which has been described by a conditional cooperativity model (21, 22, 25, 26). Another key functional difference between RelB–RelE and DinJ–YafQ is that while there is substantial evidence of conditional cooperativity regulation at *relO*, *dinJ* is not regulated by cooperative binding of DinJ–YafQ complexes at adjacent operator repeats with DinJ alone capable of transcriptionally repressing in the absence of YafQ (11). Furthermore, transcription of *dinJyafQ* is repressed by DinJ dimer or DinJ–YafQ binding to a single IR, whereas full transcriptional repression of *relBrelE* requires binding of two $RelB_2$–$RelE_2$ complexes to both IRs (11, 23). We find that truncations in the RelB C terminus that disrupt its ability to bind RelE reduce transcriptional repression at *relO* providing supporting its regulation by conditional cooperativity. Since AF3 models suggest structural differences between how each TA recognizes its operator (Fig. 6), it will be important to reconcile how each TA specifically recognizes its operator using experimental structural biology approaches.

To activate TA systems, cellular proteases degrade antitoxins, which then allows for free toxin to inhibit cellular processes (3). The (p)ppGpp alarmone is known to activate proteases providing some connection to how the RelB antitoxin may be selectively degraded (14, 46). We identified that L4 and L5 in RelB are accessible to proteases, and we predict that these regions could serve as targets for cellular proteases, thus leading to RelE toxin accumulation. We show that proteolysis at L3, which removes all α3, L4, and α4, results in a more severe growth defect. Furthermore, proteolysis at L3 and L4 was not complete indicating that these loops are not completely accessible. In the case of DinJ–YafQ, TEV recognition sites at both L5 and L3 show a growth defect reflecting the identification of only nine DinJ C-terminal residues contributing to suppression of YafQ (11). This difference may be due to additional RelB–RelE binding interfaces that could contribute to its stability beyond the α4–L4 interface. Recent studies have highlighted the role of conformational change of either the DNA repressive operator proposed to be required for transcriptional repression or the conformational change of the TA complex itself in the case of conditional cooperativity and even toxin activation (39, 45, 47–50). This work builds on these studies to identify different regions of antitoxins that are important for both sequestering its cognate toxin and transcriptional repression and that could mediate conformational changes required for conditional cooperativity.

Experimental procedures

Strains and plasmids

E. coli BL21(DE3) were used for expression of His_6-RelB, His_6-RelBΔ70–79, His_6-RelBΔ66–79, and His_6-RelBΔ19–21–RelE. The His_6-RelBΔ19–21–RelE variant was previously described where the RelBΔ19–21 variant is thought to reduce the affinity between RelB and RelE and allow for their separate purification (51) (Table S1). *E. coli* BW25113 were used for all growth assays, β-gal assays, and immunoblots. The pBAD33.1-RelB–RelE or pBAD33-FLAG-RelB–RelE plasmids served as a template for all mutagenesis experiments for RelB and RelB–RelE variants used in growth assays, β-gal assays, and immunoblots (Table S2). All point mutations were verified by Sanger sequencing. The pRK793 plasmid encoding TEV protease with kanamycin resistance was previously described (24).

Growth assays

E. coli BW25113 transformed with either pBAD33.1-RelB–RelE, pBAD33.1-RelB–RelE, or pBAD33.1-RelE variants were grown in Lysogeny broth (LB) supplemented with 25 μg ml^{-1} chloramphenicol at 37 °C. For growth curves, overnight cultures were used to inoculate (1:100 dilution) 2 ml of LB supplemented with 25 μg ml^{-1} chloramphenicol and either 0.2% L-arabinose or equivalent volume of milliQ water. The resulting cultures were grown in a 24-well plate sealed with a gas permeable sealing membrane (Breathe-Easy), incubated with shaking at 37 °C for 5 h in a BioTek Cytation5, and the absorbance was measured at 600 nm every 10 min.

For spot dilution assays, *E. coli* BW25113 transformed with pBAD33.1-RelB–RelE, pBAD33.1-RelB–RelE, or pBAD33.1-RelE variants were grown overnight in LB supplemented with 25 μg ml^{-1} chloramphenicol at 37 °C until saturation (absorption of at least 1 at 600 nm). Each culture was split in half, pelleted by centrifugation, and washed with sterile 1× PBS. After three washes, the cell pellet was resuspended in 1× PBS to an absorbance of 1 at 600 nm. Each resuspension was serial diluted 1:10 in 1X PBS and spotted on M9 agar plates supplemented with 0.1% casamino acids, 2 mM $MgSO_4$, 0.1 mM $CaCl_2$, 0.2% arabinose, 25 μg ml^{-1} chloramphenicol, and 0.4% glycerol (for induction). All were incubated at 37 °C.

For growth assays to determine accessibility of RelB L3 and L4 to TEV protease, *E. coli* BW25113 cotransformed with either pBAD33.1-RelB-L3-TEV–RelE, pBAD33.1-RelB-L4-TEV–RelE, pBAD33.1-RelB–RelE, or pBAD33.1-RelE and pRK793-MBP-TEV were grown in LB supplemented with 25 μg ml^{-1} chloramphenicol and 50 μg ml^{-1} kanamycin at 37 °C overnight with shaking. Fresh LB (2 ml) supplemented with antibiotic was inoculated (1:100 dilution) with overnight cultures. The resulting cultures were added to a 24-well plate and grown at 37 °C with shaking until an absorbance of ∼0.18 at 600 nm in a BioTek Cytation5. Expression was induced with either 0.2% L-arabinose or equivalent volume of milliQ water as a control. Cultures were grown at 37 °C with shaking for 1.5 h, expression of TEV was induced with 1 mM IPTG or equivalent volume of milliQ water as a control. The 24-well plate was sealed with a gas permeable sealing membrane (Breathe-Easy) and incubated with shaking at 37 °C for 9 h in a BioTek Cytation5, and the absorbance at 600 nm was measured every 10 min.

RelE, RelB, and RelB variant purification

To purify RelB, RelBΔ70–79, and RelBΔ66–79 proteins, we used a construct from the Strobel laboratory where the

initiator start codon of RelE was mutated to isoleucine (51). *E. coli* BL21 Gold (DE3) transformed with pET22b-His_6RelB–RelE–M1I (51), pET22b-His_6RelBΔ70–79-RelE–M1I, or pET22b-His_6RelBΔ66-79-RelE–M1I were grown in LB at 37 °C and induced with 1 mM IPTG at midlog phase. After 3 h, cells were harvested by centrifugation and the cell pellet was resuspended in lysis buffer (50 mM NaH_2PO_4, pH 8, 300 mM NaCl, 10 mM imidazole, 5 mM β-mercaptoethanol [β-Me], 0.1 mM PMSF, 0.5 mM benzamidine) and lysed *via* an Emulsiflex. The lysate was cleared by centrifugation, filtered through a 0.45-μm membrane filter, and loaded onto a 1 ml HisTrap HP Ni^{2+}-Sepharose column equilibrated with binding buffer (50 mM NaH_2PO_4, pH 8, 300 mM NaCl, 35 mM imidazole, and 5 mM β-Me), and the protein was eluted with a linear gradient of 35 to 500 mM imidazole. Fractions containing protein were pooled and dialyzed into storage buffer (50 mM NaH_2PO_4, pH 8, 150 mM NaCl, 20% glycerol, 7 mM $MgCl_2$, and 1 mM DTT), concentrated, flash-frozen in liquid nitrogen, and stored at −80 °C.

For RelE purification, *E. coli* BL21 Gold (DE3) transformed with pET22b-RelBΔ19–21–RelE were grown in LB at 37 °C and induced with 1 mM IPTG at midlog phase. After 3 h, cells were harvested by centrifugation. The cell pellet was resuspended in lysis buffer (50 mM NaH_2PO_4, pH 8, 300 mM NaCl, 10 mM imidazole, 5 mM β-Me, 0.1 mM PMSF, and 0.5 mM benzamidine) and lysed *via* an Emulsiflex. The lysate was cleared by centrifugation, filtered through a 0.45-μm membrane filter, and applied to a 5 ml HisTrap FF Crude Ni^{2+}-Sepharose column equilibrated with binding buffer (50 mM NaH_2PO_4, pH 8, 300 mM NaCl, 35 mM imidazole, and 5 mM β-Me). The RelBΔ19–21–RelE complex was eluted from the column *via* a linear gradient of 35 to 500 mM imidazole, and the fractions containing the protein were pooled and dialyzed into binding buffer. The complex was then reapplied to a 5 ml HisTrap FF Crude Ni^{2+}-Sepharose column equilibrated with binding buffer, and a linear gradient of 0 to 6 M guanidine–HCl was applied to elute RelE from the complex. Fractions containing RelE were pooled and dialyzed in refolding buffer A (50 mM bicine [pH 8.4] and 6 M guanidine–HCl) for 3 h and dialyzed in refolding buffer B (50 mM Tris–HCl, pH 7.5, 70 mM NH_4Cl, 300 mM KCl, 7 mM $MgCl_2$, 1 M guanidine–HCl, and 1 mM DTT) for an additional 3 h. RelB was then refolded on the column with a reverse linear gradient of 6-0 M guanidine–HCl and eluted with a 35 to 250 mM imidazole linear gradient. Refolded RelB and RelE were dialyzed into storage buffer (50 mM Tris–HCl, pH 7.5, 70 mM NH_4Cl, 300 mM KCl, 7 mM $MgCl_2$, 20% glycerol, and 1 mM DTT), concentrated, flash frozen in liquid nitrogen, and stored at −80 °C.

RelB–RelE and RelB variants—RelE binding assays

Covalent labeling of lysine residues of RelE (RelE has 11) was performed using the Protein Labeling Kit RED-NHS 2nd Generation from NanoTemper. Purified RelE was buffer exchanged into PBS-P (1X sterile PBS supplemented with 0.01% Pluronic F-127) and diluted to a final concentration of 20 μM. A sixfold molar excess of dye was resuspended in PBS-P and incubated with 20 μM RelE for ∼45 min in the dark at room temperature. Unreacted dye was removed using the provided B-column, a small size-exclusion column. Protein concentration was measured at 280 and 650 nm. Degree of labeling was calculated, and initial fluorescence scans were performed on the Monolith Instrument (NanoTemper). RelE with greater than 50% labeling was used in binding assays.

Labeled RelE was further diluted to a working concentration of 20 nM in assay buffer (1X sterile PBS supplemented with 0.01% Pluronic F-127). The concentration of ligand varied depending on the RelB variant, and the final concentration of labeled RelE was 10 nM. Each dilution series was incubated for at least 30 min in the dark before loading into premium capillaries to be read on the Monolith. Spectral shift measurements were performed at 25 °C. Ratios of fluorescence intensities at 670 and 650 nm were calculated within the Monolith MO control software. Negative controls included testing fluorescently labeled RelE in buffer alone and fluorescently labeled RelE incubated with an excess of unlabeled RelE, both of which showed no changes in fluorescence. Exported data were plotted in GraphPad Prism (GraphPad Software, Inc), and EC_{50} values were calculated with a binding model of agonist *versus* response variable slope. Each EC_{50} value was calculated from a total of four technical replicates from two separate protein preparations and labeling reactions.

Transcriptional repressor assays

β-gal activity assays were performed as previously described (52). *E. coli* BW25113 transformed with pOU254–*relO* or cotransformed with pOU254–*relO* and either pBAD33.1-RelB–RelE–R81A or pBAD33.1-RelB–RelE–R81A variants were grown in LB supplemented with 25 μg ml^{-1} chloramphenicol and 30 μg ml^{-1} ampicillin at 37 °C overnight with shaking. The next morning each strain was diluted 1:100 in LB supplemented with 25 μg ml^{-1} chloramphenicol, 30 μg ml^{-1} ampicillin, and 0.2% arabinose and grown with shaking at 37 °C. After 2 h, 1 ml of cells were permeabilized with 30 μl 0.1% SDS, 40 μl chloroform, and 830 μl Z-buffer. Upon *ortho*-nitrophenyl-*B*-D-galactopyranoside addition, *ortho*-nitrophenyl-*B*-D-galactopyranoside hydrolysis was measured every 1.25 min over a total of 45 min. Miller units were calculated and normalized based on the number of cells determined by absorbance at 600 nm. Degree of repression was calculated as a percentage by calculating the decrease in Miller units from cells carrying plasmid-encoded RelB (or its variants) and RelE compared with cells lacking any plasmid-encoded RelB–RelE proteins (*e.g.*, pOU254–*relO*).

Transcriptional repression via *RT–qPCR*

RNA was prepared from *E. coli* BW25113 transformed with pOU254–*relO* alone or cotransformed with pOU254–*relO* and either pBAD33.1-RelB–RelE–R81A or pBAD33.1-RelB–RelE–R81A variants grown in LB supplemented with 25 μg ml^{-1} chloramphenicol and 30 μg ml^{-1} ampicillin and 0.2% arabinose at 37 °C for 2 h. RNA was extracted as

described by New England Biolabs Monarch Total RNA miniprep kit for TRIzol-extracted samples. Extracted RNA was treated with Turbo DNase for 20 min at 37 °C, and then phenol–chloroform was extracted. Complementary DNA was generated following the ProtoScript II Reverse Transcriptase protocol and treated with RNase H. RT–qPCR was performed with primers to *lacZ*, and *rpoD* was the internal control (Table S2). Relative levels of RNA were calculated using the ΔΔCT method relative to construct with wildtype RelB–RelE–R81A expression. Data are the averages from three independent biological replicates ± SD.

Immunoblot analysis of RelB and RelB variants

E. coli BW25113 transformed with either pBAD33-FLAG-RelB–RelE wildtype or pBAD33-FLAG-RelB–RelE variants were grown in LB supplemented with 25 μg ml^{-1} chloramphenicol at 37 °C overnight with shaking. Overnight cultures were diluted 1:100 in fresh LB supplemented with 25 μg ml^{-1} chloramphenicol and 0.2% L-arabinose. Cultures were grown at 37 °C with shaking for 3 h, the absorbance at 600 nm was measured, cultures were pelleted *via* centrifugation, and flash frozen in liquid nitrogen.

Cell pellets were resuspended in lysis buffer (20 mM Tris–HCl, pH 7.5, 250 mM KCl, 0.1% Triton X-100, 5 mM β-Me, 0.1 mM benzamidine, and 0.1 mM PMSF) to an absorbance at 600 nm of 0.5. Resuspended cells were lysed *via* 10 cycles of freeze and thaw. After lysis, cells were pelleted by centrifugation with the lysate in the soluble fraction. Total protein concentration in the soluble lysate was determined *via* Bradford assay. Total protein (5 μg) was mixed with 2X Laemmli buffer (40% glycerol, 125 mM Tris–HCl, 4% SDS, 0.05% bromophenol blue, and 0.05% β-Me) and loaded on an 8 to 16% Invitrogen Novex Tris–Glycine Mini Protein Gel. Proteins were resolved and then transferred to a nitrocellulose membrane. Membrane was blocked with 5% milk in 1X Tris-buffered saline with 0.1% Tween-20 for 1 h at room temperature with shaking. Membrane was probed with 1:5000 dilution of Sigma–Aldrich Monoclonal anti-FLAG M2 for 30 min and subsequently incubated with 1:15,000 dilution of anti-mouse–conjugated to horseradish peroxidase (HRP). Membrane was incubated with room temperature Immobilon Classico Western HRP substrate, and chemiluminescence was detected by a BioRad ChemiDoc. As a loading control, the membrane was then probed for maltose-binding protein (MBP) with a 1:5000 dilution of rabbit anti-MBP for 30 min and subsequently incubated with 1:15,000 dilution goat anti-rabbit secondary conjugated to HRP. Membrane was incubated in room temperature with Immobilon Classico Western HRP substrate, and chemiluminescence was detected by a Bio-Rad ChemiDoc.

Identification of proteolyzed RelB

E. coli BW25113 cotransformed with either pBAD33.1-His_6-RelB-L3-TEV–RelE or pBAD33.1-His_6-RelB–L4-TEV–RelE and pRK793-MBP-TEV were grown overnight in LB at 37 °C with 25 μg ml^{-1} chloramphenicol and 50 μg ml^{-1} kanamycin. Overnight cultures were diluted 1:100 in fresh LB supplemented with 25 μg ml^{-1} chloramphenicol, 50 μg ml^{-1} kanamycin, and 0.2% L-arabinose. After 2 h, cells were induced with 1 mM IPTG, grown for 1.5 h, and harvested by centrifugation. The pellet was resuspended in lysis buffer (20 mM Tris–HCl, pH 7.5, 250 mM KCl, 0.1% Triton X-100, 5 mM β-Me, 0.1 mM benzamidine, and 0.1 mM PMSF) and lysed *via* 10 cycles of freeze and thaw. After lysis, cells were pelleted by centrifugation, and the lysate was applied to a equilibrated NEBExpress Ni^{2+} Spin Column and purified following the NEB Express Ni^{2+} Spin Column Quick Start Protocol, with two minor changes. These changes are that the lysate was incubated with resin for 5 min at 4 °C with agitation, and resin was washed five times with wash buffer. Eluted proteins were mixed with 2X Laemmli buffer (40% glycerol, 125 mM Tris–HCl, 4% SDS, 0.05% bromophenol blue, and 0.05% β-Me) and run on a 20% SDS-PAGE and stained with Coomassie G-250. Bands corresponding to TEV-proteolyzed RelB-L4-TEV or RelB-L3-TEV were gel extracted. Proteins were extracted by destaining with destaining solution (50% acetonitrile), followed by gel dehydration with 100% acetonitrile, and an overnight incubation of dehydrated gel with extraction buffer (50% formic acid, 25% acetonitrile, and 15% isopropanol) at 37 °C with agitation. The next morning, mixtures were centrifuged and the supernatant containing extracted protein was isolated. Extracted protein was buffer exchanged into 0.1% formic acid.

Chromatographic separation was performed using a Thermo Fisher Scientific Vanquish Neo UHPLC system coupled with an EASY-Spray HPLC column (ES907, 150 mm × 150 μm, 4 μm particle size, polystyrene–divinylbenzene packing material; Thermo Fisher Scientific). The column temperature was maintained at 60 °C to optimize protein elution and ensure stable spray performance, as recommended for EASY-Spray columns. A 10 min linear gradient was employed, with mobile phase A consisting of 0.1% formic acid in water and mobile phase B consisting of 0.1% formic acid in 80% acetonitrile. The gradient ranged from 5% to 55% B over 10 min at a flow rate of 2 μl min^{-1}, suitable for the capillary flow design of the ES907 column. The injection volume was 15 μl, corresponding to 100 mM of protein loaded onto the column. A 2 min column re-equilibration at 1% B was included postgradient.

Intact protein analysis was conducted on a Thermo Fisher Scientific Orbitrap Exploris 480 mass spectrometer equipped with an Easy Spray Ionization source, optimized for the EASY-Spray column's integrated fused-silica emitter. The instrument was operated in positive ion mode with the following source parameters: spray voltage, 1.8 kV; on transfer tube temperature, 32 °C. Full mass spectrometry scans were acquired in the *m/z* range of 500 to 2000 at a resolution of 240,000 (at *m/z* 200). The automatic gain control target was set to 3e6 ions with a maximum injection time of 100 ms. Raw mass spectra were processed using Thermo Fisher Scientific Free Style software (version 1.8). Deconvolution of the intact protein mass spectra was performed using freestyle. The resulting deconvoluted spectra were manually inspected to confirm the presence of the expected molecular weight.

AF3 structure predictions

Amino acid sequences of RelB, RelE, DinJ, and YafQ were obtained from Kyoto Encyclopedia of Genes and Genomes. The *relBrelE* DNA operator site (*relO*) and the *dinJyafQ* DNA operator site (*dinJ*) were previously determined (11, 25). Using AF3 (44), 3D complex structures of the RelB–RelE heterotetramer bound to *relO* containing a single IR (12 nts) and the DinJ–YafQ heterotetramer bound to *dinJ* containing a single IR (9 nts) were assessed.

Data availability

Most data are available in the article. The mass spectrometry proteomics data have been deposited to the ProteomeXchange Consortium via the Pride[1] partner repository with the data identifier PXD065338.

Supporting information—This article contains supporting information (24, 25, 51, 53, 54).

Acknowledgments—We acknowledge the Systems Mass Spectrometry Core at the Institute of Bioengineering and Bioscience, Georgia Institute of Technology, and specifically Lebon Ludyanna and Dr Rakesh Singh. We thank the Strobel laboratory for the pET-RelB–RelE–M1I plasmid and the Gerdes laboratory for the pOU254 plasmid.

Author contributions—J. T., I. J. P., and C. M. D. conceptualization; J. T. methodology; J. T., I. J. P., M. G., and C. M. D. formal analysis; J. T. and I. J. P. investigation; C. M. D. resources; J. T. and I. J. P. data curation; J. T. and C. M. D. writing–original draft; J. T., I. J. P., M. P., and C. M. D. writing–review & editing; M. G. and C. M. D. supervision; C. M. D. project administration; J. T. and C. M. D. funding acquisition.

Funding and additional information—We thank Dr Graeme Conn for critical reading of the article. Support for this work was provided by the National Institutes of Health (NIH) R01 GM093278 (to C. M. D.), NIH R35 GM156629 (to C. M. D.), NIH R35 GM133509 (to M. G.), National Science Foundation GRFP 2021310209 (to J. T.), and NIH T32 GM135060-01 (to J. T.). C. M. D. is a Burroughs Wellcome Fund Investigator in the Pathogenesis of Infectious Diseases. The content is solely the responsibility of the authors and does not necessarily represent the official views of the NIH.

Conflict of interest—The authors declare that they have no conflicts of interest with the contents of this article.

Abbreviations—The abbreviations used are: AF3, AlphaFold 3; CI, confidence interval; β-gal, β-galactosidase; β-Me, β-mercaptoethanol; HRP, horseradish peroxidase; IR, inverted repeat; L3, loop 3; L4, loop 4; L5, loop 5; LB, Lysogeny broth; MBP, maltose-binding protein; NIH, National Institutes of Health; qPCR, quantitative PCR; TA, toxin–antitoxin; TEV, tobacco etch virus.

References

1. Page, R., and Peti, W. (2016) Toxin-antitoxin systems in bacterial growth arrest and persistence. *Nat. Chem. Biol.* **12**, 208–214
2. Harms, A., Brodersen, D. E., Mitarai, N., and Gerdes, K. (2018) Toxins, targets, and triggers: an overview of toxin-antitoxin biology. *Mol. Cell* **70**, 768–784
3. Jurenas, D., Fraikin, N., Goormaghtigh, F., and Van Melderen, L. (2022) Biology and evolution of bacterial toxin-antitoxin systems. *Nat. Rev. Microbiol.* **20**, 335–350
4. Lehnherr, H., Maguin, E., Jafri, S., and Yarmolinsky, M. B. (1993) Plasmid addiction genes of bacteriophage P1: doc, which causes cell death on curing of prophage, and phd, which prevents host death when prophage is retained. *J. Mol. Biol.* **233**, 414–428
5. Pandey, D. P., and Gerdes, K. (2005) Toxin-antitoxin loci are highly abundant in free-living but lost from host-associated prokaryotes. *Nucleic Acids Res.* **33**, 966–976
6. Fozo, E. M., Makarova, K. S., Shabalina, S. A., Yutin, N., Koonin, E. V., and Storz, G. (2010) Abundance of type I toxin-antitoxin systems in bacteria: searches for new candidates and discovery of novel families. *Nucleic Acids Res.* **38**, 3743–3759
7. Blower, T. R., Short, F. L., Rao, F., Mizuguchi, K., Pei, X. Y., Fineran, P. C., *et al.* (2012) Identification and classification of bacterial Type III toxin-antitoxin systems encoded in chromosomal and plasmid genomes. *Nucleic Acids Res.* **40**, 6158–6173
8. LeRoux, M., and Laub, M. T. (2022) Toxin-antitoxin systems as phage defense elements. *Annu. Rev. Microbiol.* **76**, 21–43
9. Li, M., Gong, L., Cheng, F., Yu, H., Zhao, D., Wang, R., *et al.* (2021) Toxin-antitoxin RNA pairs safeguard CRISPR-Cas systems. *Science* **372**, eabe5601
10. Papadakos, G., Wojdyla, J. A., and Kleanthous, C. (2012) Nuclease colicins and their immunity proteins. *Q. Rev. Biophys.* **45**, 57–103
11. Ruangprasert, A., Maehigashi, T., Miles, S. J., Giridharan, N., Liu, J. X., and Dunham, C. M. (2014) Mechanisms of toxin inhibition and transcriptional repression by Escherichia coli DinJ-YafQ. *J. Biol. Chem.* **289**, 20559–20569
12. Christensen, S. K., Mikkelsen, M., Pedersen, K., and Gerdes, K. (2001) RelE, a global inhibitor of translation, is activated during nutritional stress. *Proc. Natl. Acad. Sci. U. S. A* **98**, 14328–14333
13. Christensen, S. K., and Gerdes, K. (2003) RelE toxins from bacteria and Archaea cleave mRNAs on translating ribosomes, which are rescued by tmRNA. *Mol. Microbiol.* **48**, 1389–1400
14. Sorensen, M. A. (2001) Charging levels of four tRNA species in Escherichia coli Rel(+) and Rel(−) strains during amino acid starvation: a simple model for the effect of ppGpp on translational accuracy. *J. Mol. Biol.* **307**, 785–798
15. Christensen, S. K., and Gerdes, K. (2004) Delayed-relaxed response explained by hyperactivation of RelE. *Mol. Microbiol.* **53**, 587–597
16. Zhao, Y., McAnulty, M. J., and Wood, T. K. (2016) Toxin YafQ reduces Escherichia coli growth at low temperatures. *PLoS One* **11**, e0161577
17. Pedersen, K., Zavialov, A. V., Pavlov, M. Y., Elf, J., Gerdes, K., and Ehrenberg, M. (2003) The bacterial toxin RelE displays codon-specific cleavage of mRNAs in the ribosomal A site. *Cell* **112**, 131–140
18. Neubauer, C., Gao, Y. G., Andersen, K. R., Dunham, C. M., Kelley, A. C., Hentschel, J., *et al.* (2009) The structural basis for mRNA recognition and cleavage by the ribosome-dependent endonuclease RelE. *Cell* **139**, 1084–1095
19. Prysak, M. H., Mozdzierz, C. J., Cook, A. M., Zhu, L., Zhang, Y., Inouye, M., *et al.* (2009) Bacterial toxin YafQ is an endoribonuclease that associates with the ribosome and blocks translation elongation through sequence-specific and frame-dependent mRNA cleavage. *Mol. Microbiol.* **71**, 1071–1087
20. Maehigashi, T., Ruangprasert, A., Miles, S. J., and Dunham, C. M. (2015) Molecular basis of ribosome recognition and mRNA hydrolysis by the E. coli YafQ toxin. *Nucleic Acids Res.* **43**, 8002–8012
21. Li, G. Y., Zhang, Y., Inouye, M., and Ikura, M. (2008) Structural mechanism of transcriptional autorepression of the Escherichia coli RelB/RelE antitoxin/toxin module. *J. Mol. Biol.* **380**, 107–119
22. Boggild, A., Sofos, N., Andersen, K. R., Feddersen, A., Easter, A. D., Passmore, L. A., *et al.* (2012) The crystal structure of the intact E. coli RelBE toxin-antitoxin complex provides the structural basis for conditional cooperativity. *Structure* **20**, 1641–1648

23. Liang, Y., Gao, Z., Wang, F., Zhang, Y., Dong, Y., and Liu, Q. (2014) Structural and functional characterization of Escherichia coli toxin-antitoxin complex DinJ-YafQ. *J. Biol. Chem.* **289**, 21191–21202
24. Ruangprasert, A., Maehigashi, T., Miles, S. J., and Dunham, C. M. (2017) Importance of the E. coli DinJ antitoxin carboxy terminus for toxin suppression and regulated proteolysis. *Mol. Microbiol.* **104**, 65–77
25. Overgaard, M., Borch, J., Jorgensen, M. G., and Gerdes, K. (2008) Messenger RNA interferase RelE controls relBE transcription by conditional cooperativity. *Mol. Microbiol.* **69**, 841–857
26. Overgaard, M., Borch, J., and Gerdes, K. (2009) RelB and RelE of Escherichia coli form a tight complex that represses transcription via the ribbon-helix-helix motif in RelB. *J. Mol. Biol.* **394**, 183–196
27. Francuski, D., and Saenger, W. (2009) Crystal structure of the antitoxin-toxin protein complex RelB-RelE from Methanococcus jannaschii. *J. Mol. Biol.* **393**, 898–908
28. Gotfredsen, M., and Gerdes, K. (1998) The Escherichia coli relBE genes belong to a new toxin-antitoxin gene family. *Mol. Microbiol.* **29**, 1065–1076
29. Galvani, C., Terry, J., and Ishiguro, E. E. (2001) Purification of the RelB and RelE proteins of Escherichia coli: RelE binds to RelB and to ribosomes. *J. Bacteriol.* **183**, 2700–2703
30. Li, G. Y., Zhang, Y., Inouye, M., and Ikura, M. (2009) Inhibitory mechanism of Escherichia coli RelE-RelB toxin-antitoxin module involves a helix displacement near an mRNA interferase active site. *J. Biol. Chem.* **284**, 14628–14636
31. Mutschler, H., Reinstein, J., and Meinhart, A. (2010) Assembly dynamics and stability of the pneumococcal epsilon zeta antitoxin toxin (PezAT) system from Streptococcus pneumoniae. *J. Biol. Chem.* **285**, 21797–21806
32. Magnuson, R., and Yarmolinsky, M. B. (1998) Corepression of the P1 addiction operon by phd and doc. *J. Bacteriol.* **180**, 6342–6351
33. Gerdes, K., Christensen, S. K., and Lobner-Olesen, A. (2005) Prokaryotic toxin-antitoxin stress response loci. *Nat. Rev. Microbiol.* **3**, 371–382
34. Garcia-Pino, A., Balasubramanian, S., Wyns, L., Gazit, E., De Greve, H., Magnuson, R. D., *et al.* (2010) Allostery and intrinsic disorder mediate transcription regulation by conditional cooperativity. *Cell* **142**, 101–111
35. Cataudella, I., Trusina, A., Sneppen, K., Gerdes, K., and Mitarai, N. (2012) Conditional cooperativity in toxin-antitoxin regulation prevents random toxin activation and promotes fast translational recovery. *Nucleic Acids Res.* **40**, 6424–6434
36. Hampton, H. G., Jackson, S. A., Fagerlund, R. D., Vogel, A. I. M., Dy, R. L., Blower, T. R., *et al.* (2018) AbiEi binds cooperatively to the type IV abiE toxin-antitoxin operator via a positively-charged surface and causes DNA bending and negative autoregulation. *J. Mol. Biol.* **430**, 1141–1156
37. Qian, H., Yu, H., Li, P., Zhu, E., Yao, Q., Tai, C., *et al.* (2019) Toxin-antitoxin operon kacAT of Klebsiella pneumoniae is regulated by conditional cooperativity via a W-shaped KacA-KacT complex. *Nucleic Acids Res.* **47**, 7690–7702
38. Li, P., Goh, Y. X., Ilic, B., Tai, C., Deng, Z., Chen, Z., *et al.* (2023) Antibiotic-induced degradation of antitoxin enhances the transcription of acetyltransferase-type toxin-antitoxin operon. *J. Antimicrob. Chemother.* **78**, 1066–1075
39. Grabe, G. J., Giorgio, R. T., Wieczor, M., Gollan, B., Sargen, M., Orozco, M., *et al.* (2024) Molecular stripping underpins derepression of a toxin-antitoxin system. *Nat. Struct. Mol. Biol.* **31**, 1050–1060
40. Gronlund, H., and Gerdes, K. (1999) Toxin-antitoxin systems homologous with relBE of Escherichia coli plasmid P307 are ubiquitous in prokaryotes. *J. Mol. Biol.* **285**, 1401–1415
41. Hiller, D. A., Dunican, B. F., Nallur, S., Li, N. S., Piccirilli, J. A., and Strobel, S. A. (2020) The positively charged active site of the bacterial toxin RelE causes a large shift in the general base pK(a). *Biochemistry* **59**, 1665–1671
42. Van Melderen, L., Bernard, P., and Couturier, M. (1994) Lon-dependent proteolysis of CcdA is the key control for activation of CcdB in plasmid-free segregant bacteria. *Mol. Microbiol.* **11**, 1151–1157
43. Schureck, M. A., Meisner, J., Hoffer, E. D., Wang, D., Onuoha, N., Ei Cho, S., *et al.* (2019) Structural basis of transcriptional regulation by the HigA antitoxin. *Mol. Microbiol.* **111**, 1449–1462
44. Abramson, J., Adler, J., Dunger, J., Evans, R., Green, T., Pritzel, A., *et al.* (2024) Accurate structure prediction of biomolecular interactions with AlphaFold 3. *Nature* **630**, 493–500
45. Grabe, G. J., Giorgio, R. T., Hall, A. M. J., Morgan, R. M. L., Dubois, L., Sisley, T. A., *et al.* (2021) Auxiliary interfaces support the evolution of specific toxin-antitoxin pairing. *Nat. Chem. Biol.* **17**, 1296–1304
46. Sinha, A. K., and Winther, K. S. (2021) The RelA hydrolase domain acts as a molecular switch for (p)ppGpp synthesis. *Commun. Biol.* **4**, 434
47. Sanchez-Torres, V., Hwang, H. J., and Wood, T. K. (2024) Conformational change as a mechanism for toxin activation in bacterial toxin-antitoxin systems. *J. Virol.* **98**, e0151324
48. Burman, N., Belukhina, S., Depardieu, F., Wilkinson, R. A., Skutel, M., Santiago-Frangos, A., *et al.* (2024) A virally encoded tRNA neutralizes the PARIS antiviral defence system. *Nature* **634**, 424–431
49. Deep, A., Liang, Q., Enustun, E., Pogliano, J., and Corbett, K. D. (2024) Architecture and activation mechanism of the bacterial PARIS defence system. *Nature* **634**, 432–439
50. Beck, I. N., Arrowsmith, T. J., Grobbelaar, M. J., Bromley, E. H. C., Marles-Wright, J., and Blower, T. R. (2024) Toxin release by conditional remodelling of ParDE1 from Mycobacterium tuberculosis leads to gyrase inhibition. *Nucleic Acids Res.* **52**, 1909–1929
51. Griffin, M. A., Davis, J. H., and Strobel, S. A. (2013) Bacterial toxin RelE: a highly efficient ribonuclease with exquisite substrate specificity using atypical catalytic residues. *Biochemistry* **52**, 8633–8642
52. Marotta, J., May, K. L., Bae, C. Y., and Grabowicz, M. (2023) Molecular insights into Escherichia coli Cpx envelope stress response activation by the sensor lipoprotein NlpE. *Mol. Microbiol.* **119**, 586–598
53. Guzman, L. M., Barondess, J. J., and Beckwith, J. (1992) FtsL, an essential cytoplasmic membrane protein involved in cell division in Escherichia coli. *J. Bacteriol.* **174**, 7716–7728
54. Chung, H. S., and Raetz, C. R. (2010) Interchangeable domains in the Kdo transferases of Escherichia coli and Haemophilus influenzae. *Biochemistry* **49**, 4126–4137